Supporting Information

Multiscale Computational Prediction of β-Sheet Peptide Self-Assembly Morphology

Li Deng[a,b,c] and Yanting Wang*[d,e]

[a]BGI-Qingdao, BGI-Shenzhen, 2 Hengyunshan Road, Qingdao 266555, China

[b]State Key Laboratory of Agricultural Genomics, BGI-Shenzhen, Shenzhen 518083, China

[c]China National GeneBank, BGI-Shenzhen, Shenzhen 518120, China

[d]CAS Key Laboratory of Theoretical Physics, Institute of Theoretical Physics, Chinese Academy of Sciences, 55 East Zhongguancun Road, P. O. Box 2735, Beijing, 100190 China

[e]School of Physical Sciences, University of Chinese Academy of Sciences, 19A Yuquan Road, Beijing, 100049 China

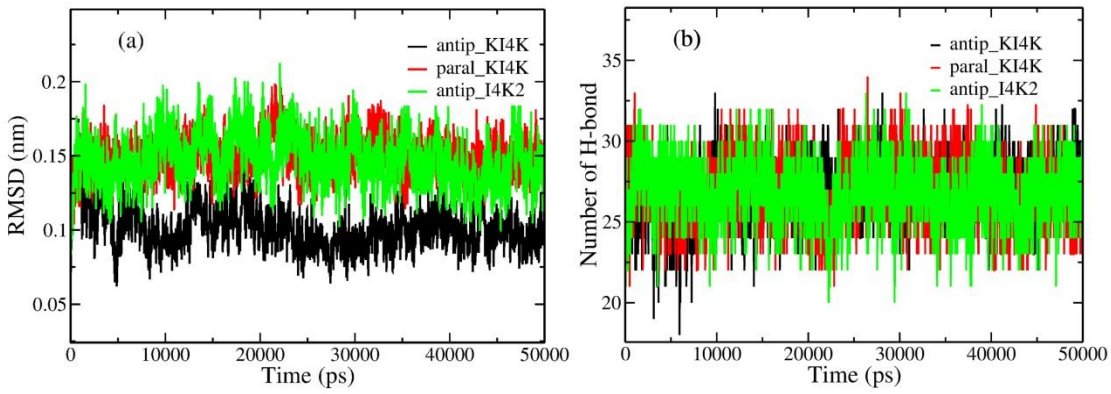

Figure S1. RMSD and number of H-bonds between peptides for different cross-β sheets in 50-ns simulations.

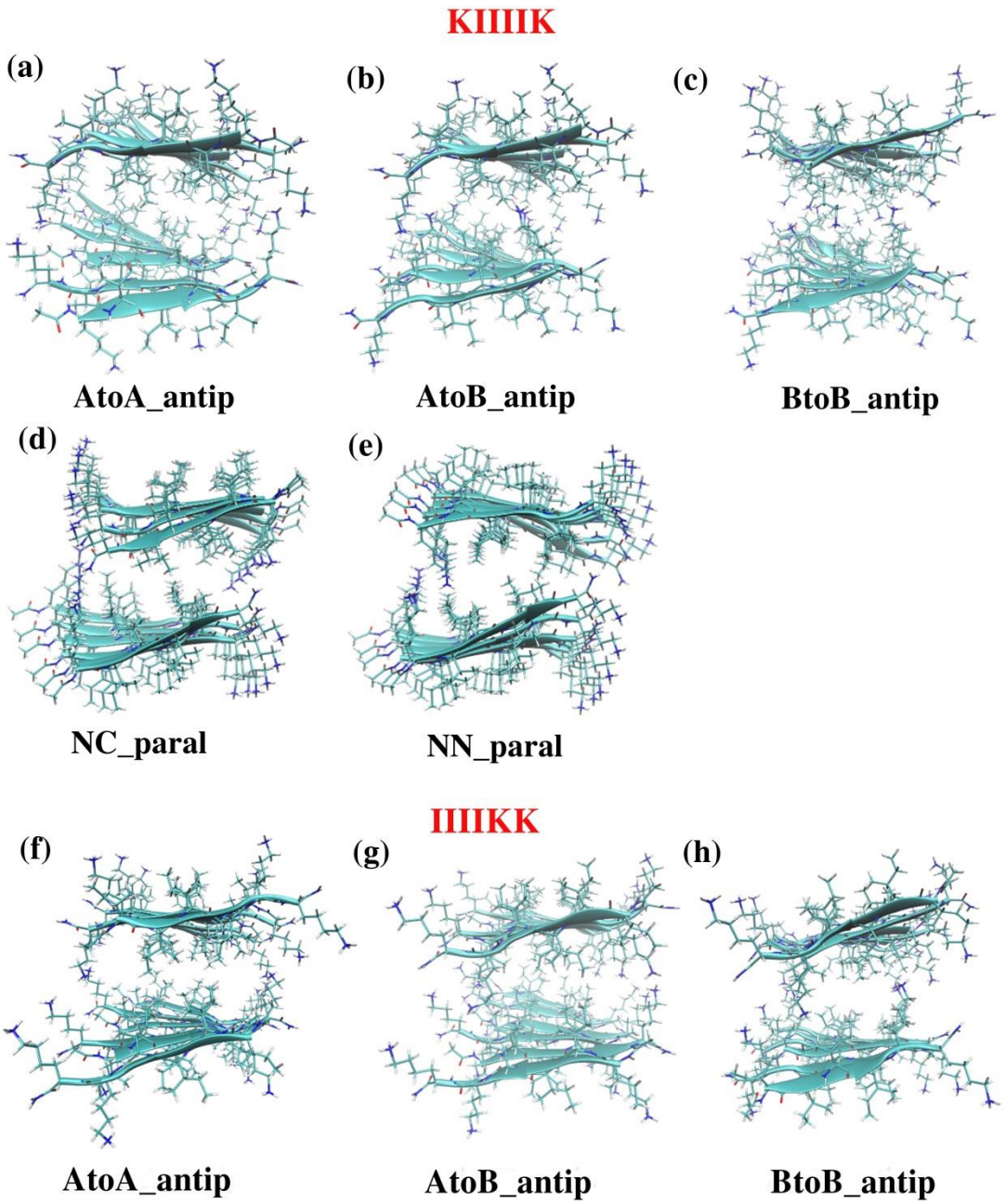

Figure S2. Initial configurations of all stacking modes of inter-sheet structures: (a), (b), (c) are inter-sheet structures of the anti-parallel cross-β sheet with face A close to face A, face A close to face B, and face B close to face B, respectively, for KI4K; (d), (e) are inter-sheet structures of the parallel cross-β sheet with side N close to side N, and side N close to side C, respectively; and (f), (g), (h) are inter-sheet structures of the anti-parallel cross-β sheet with face A close to face A, face A close to face B, and face B close to face B, respectively, for I4K2.

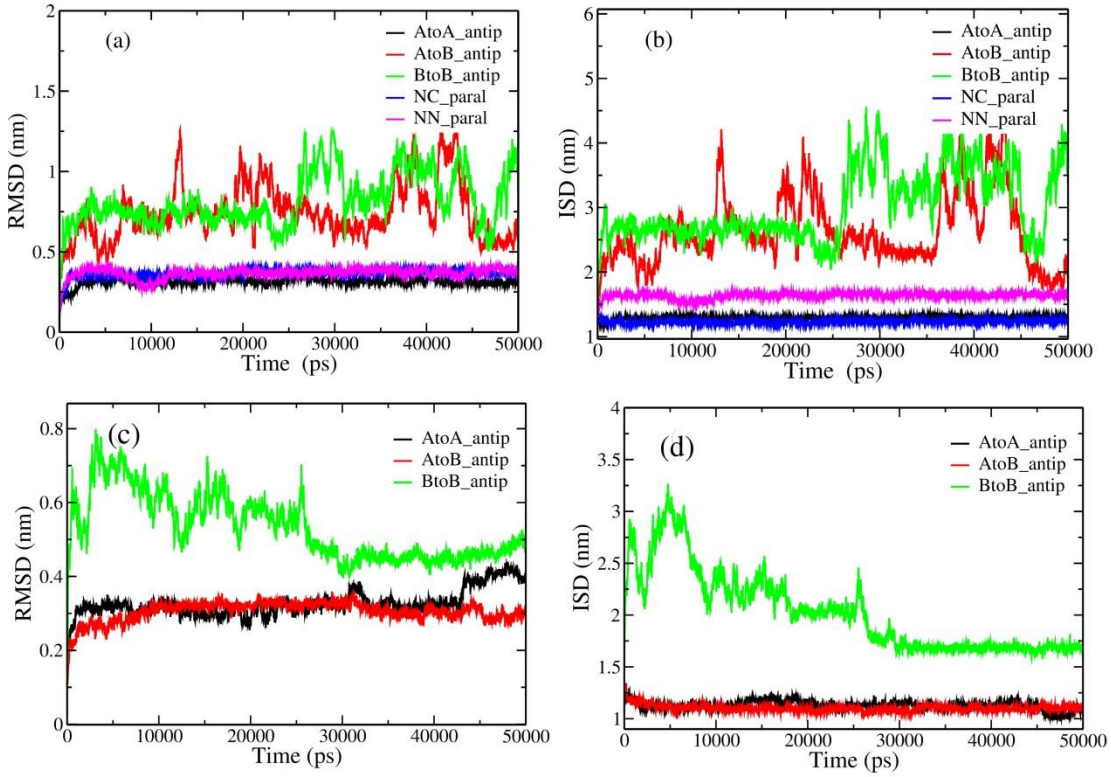

Figure S3. RMSD and ISD between two cross-β sheets for all kinds of inter-sheet structures: (a), (b) are results for KI4K, and (c), (d) are results for I4K2.

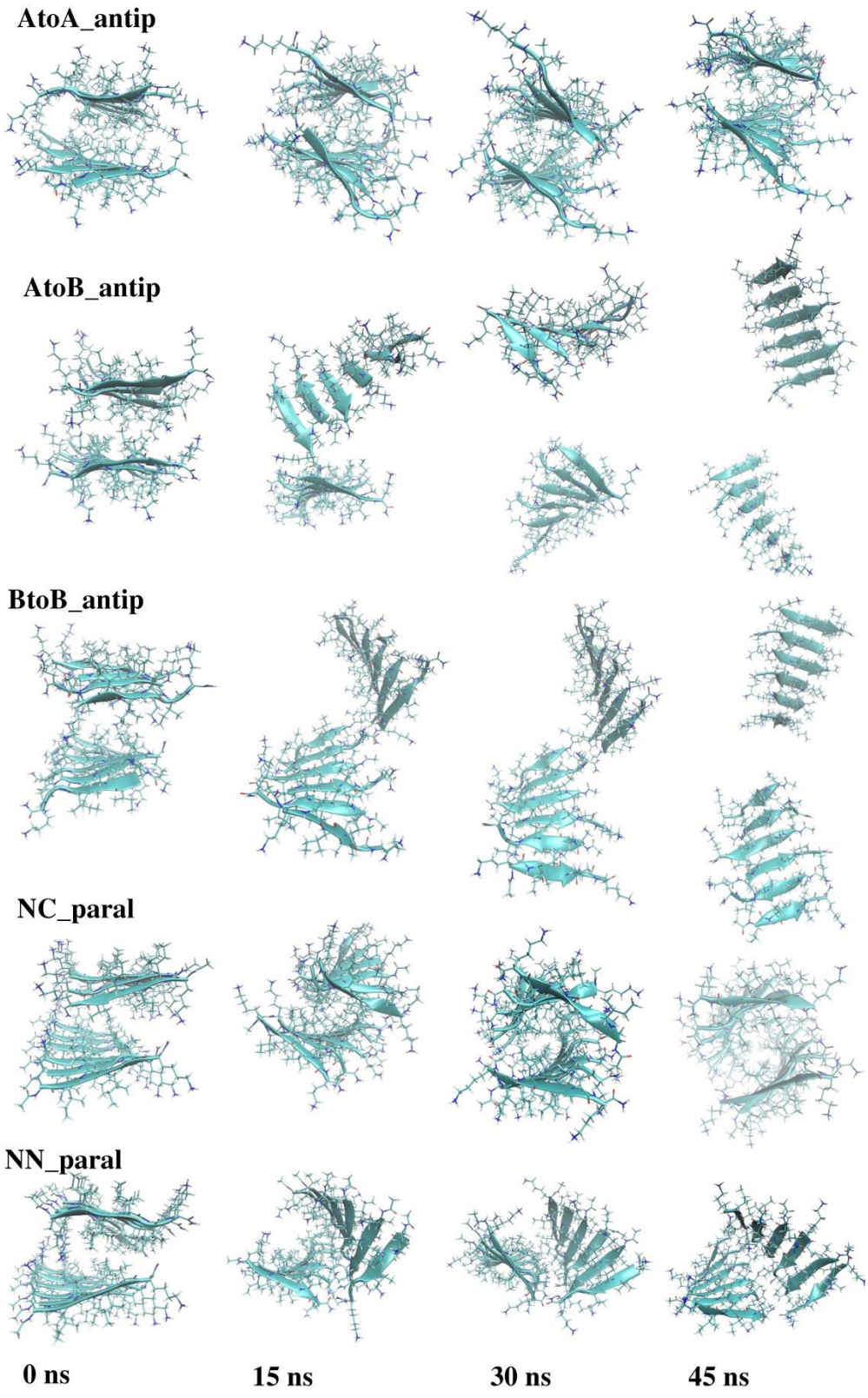

Figure S4. Snapshots of two cross-β sheets of KI4K with different packing modes evolving with time, illustrating the stabilities of the inter-sheet structures.

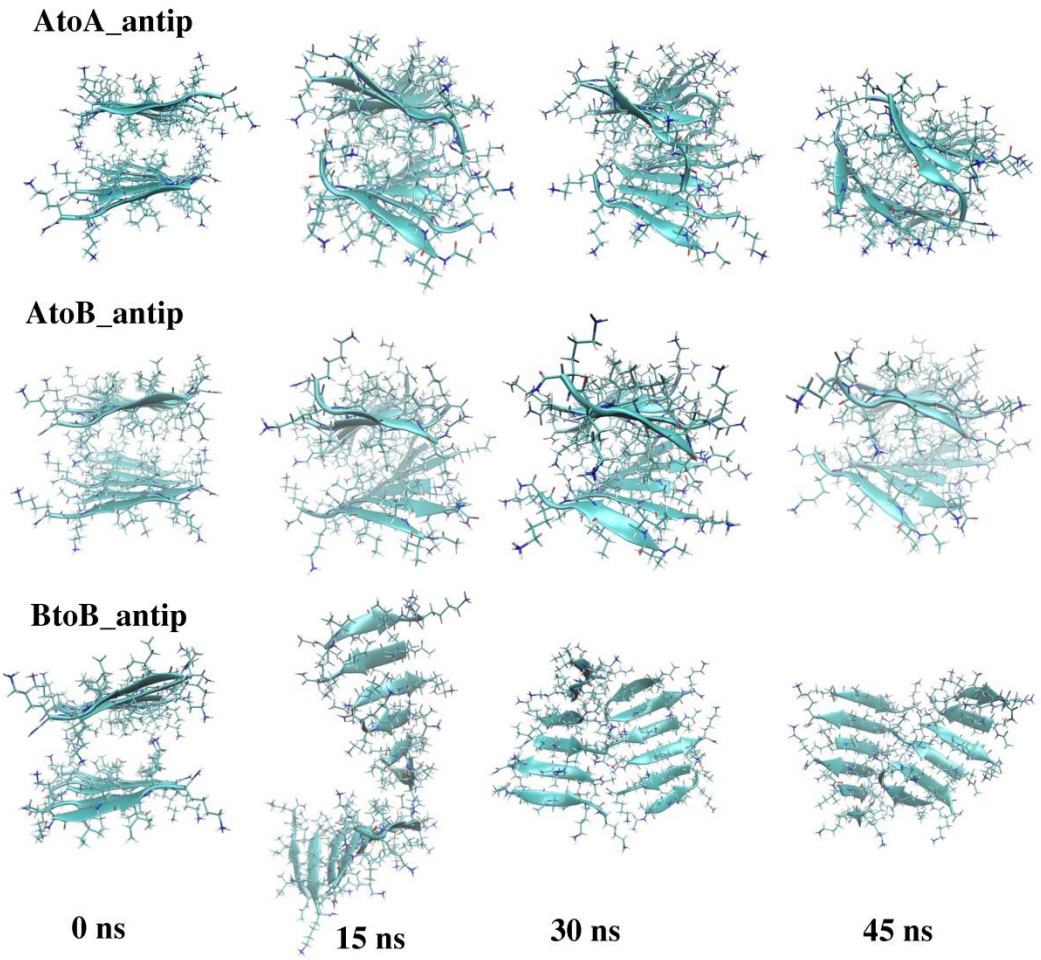

Figure S5. Snapshots of two cross-β sheets of I4K2 with different packing modes evolving with time, illustrating the stabilities of the inter-sheet structures.

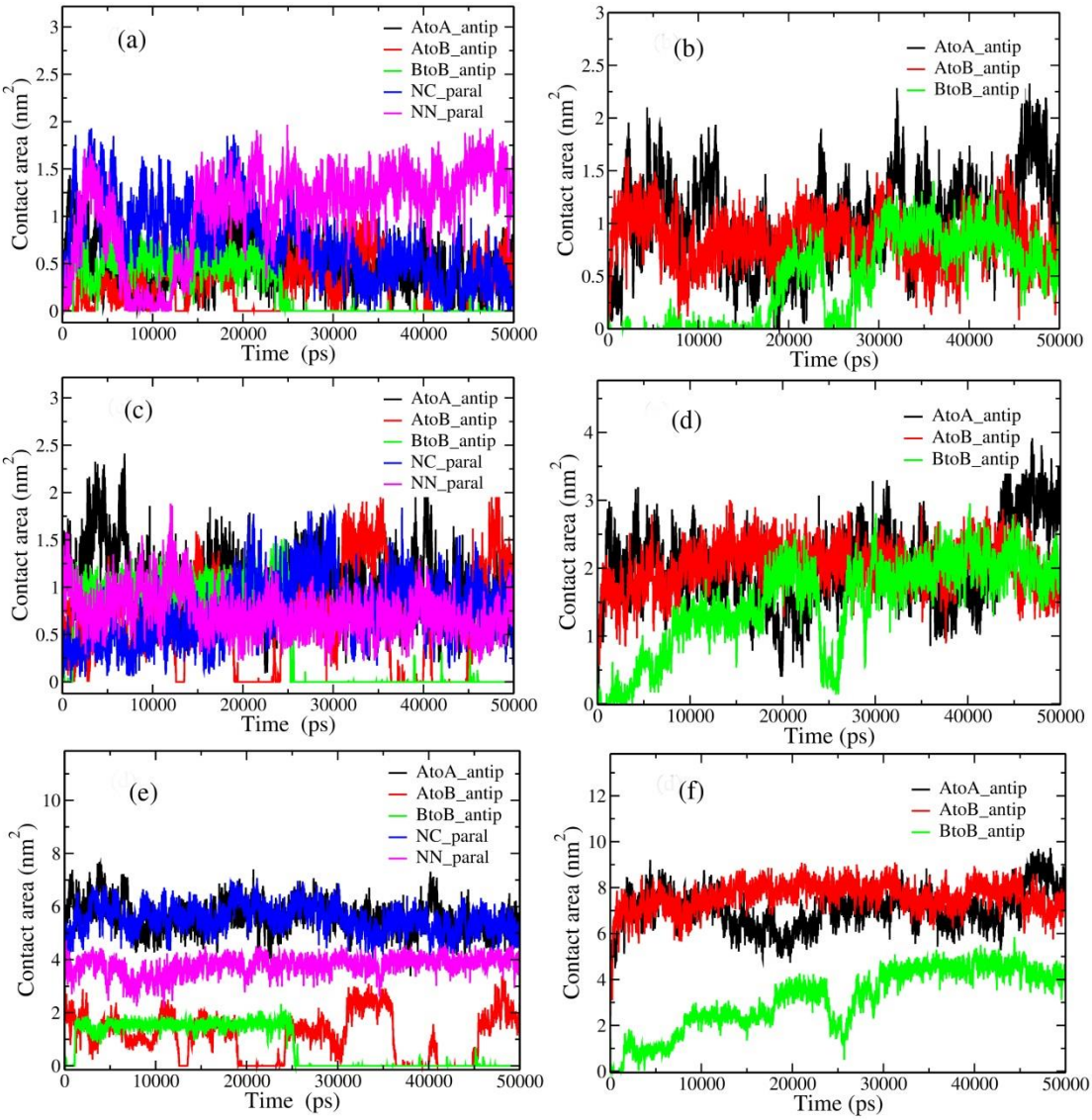

Figure S6. Contact area of all inter-sheet structures for KI4K and I4K2: hydrophilic-hydrophilic-residue contact areas in a) and b), hydrophobic-hydrophilic-residue contact areas in c) and d), and total contact areas in e) and f).

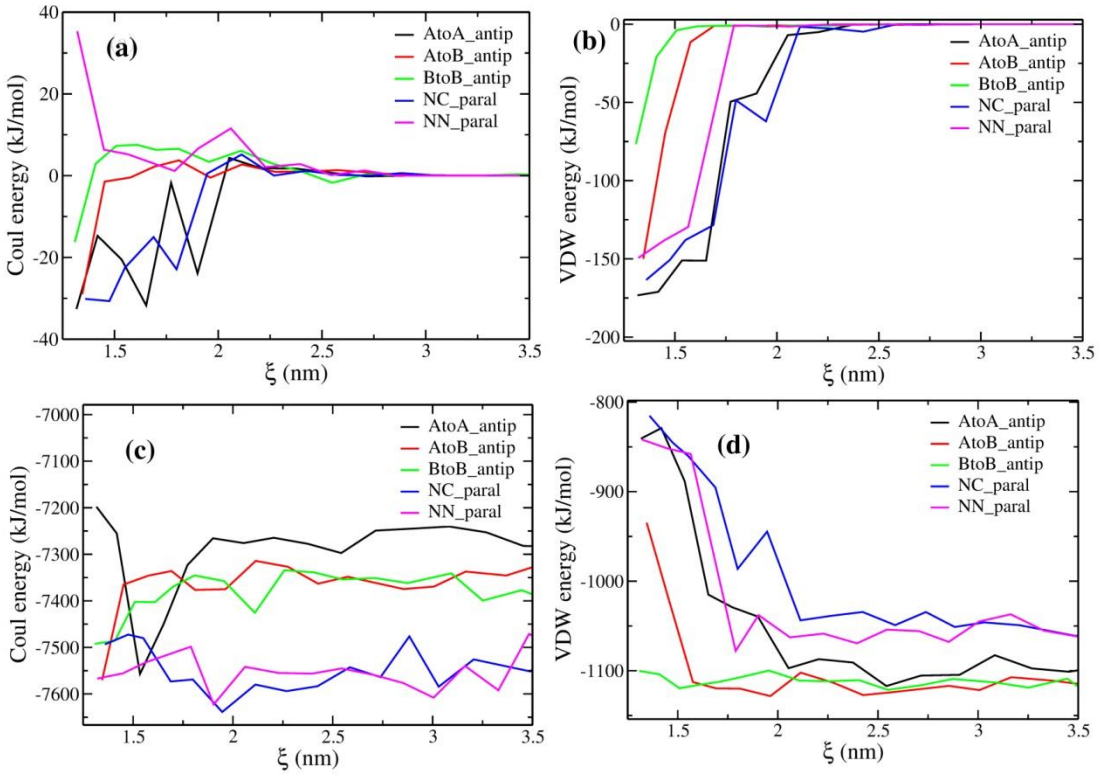

Figure S7. Energy decompositions for different inter-sheet structures of KI4K.

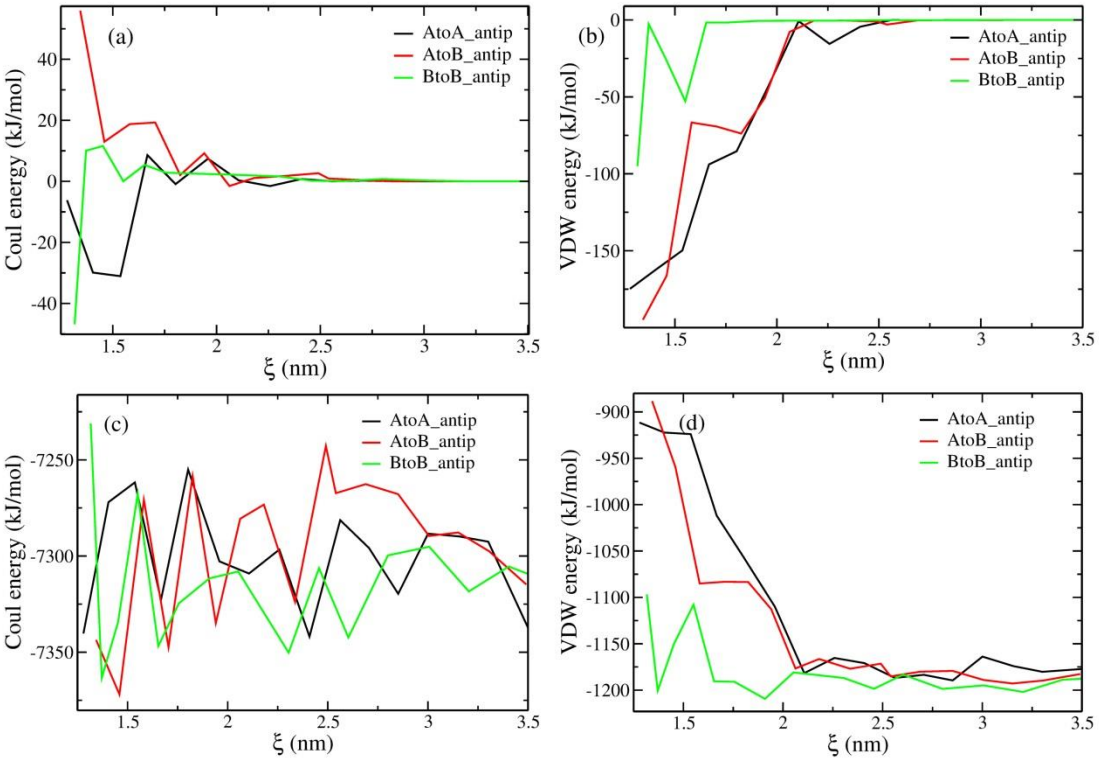

Figure S8. Energy decompositions for different inter-sheet structures of I4K2.

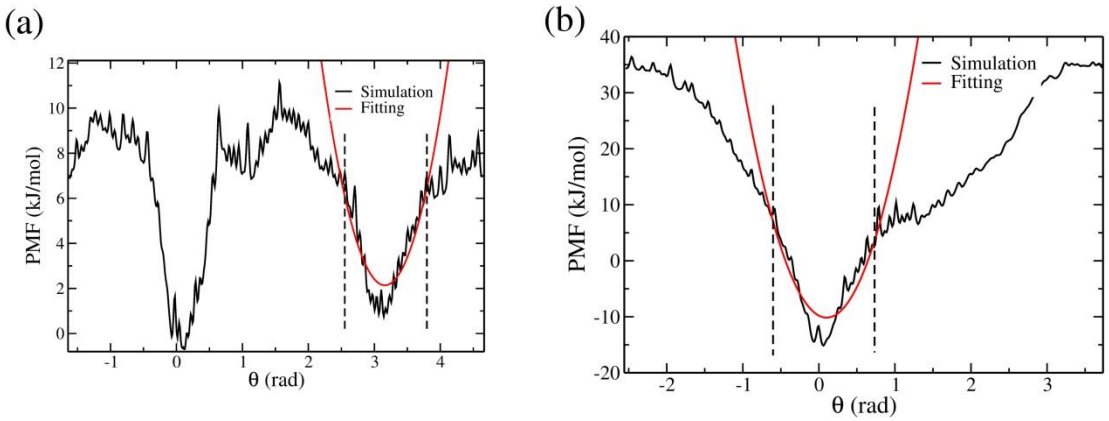

Figure S9. Total PMFs and harmonic fitting of the potential wells for the twisting strength of dimer. (a) is the parallel dimer of KI4K and (b) is the antiparallel dimer of I4K2.

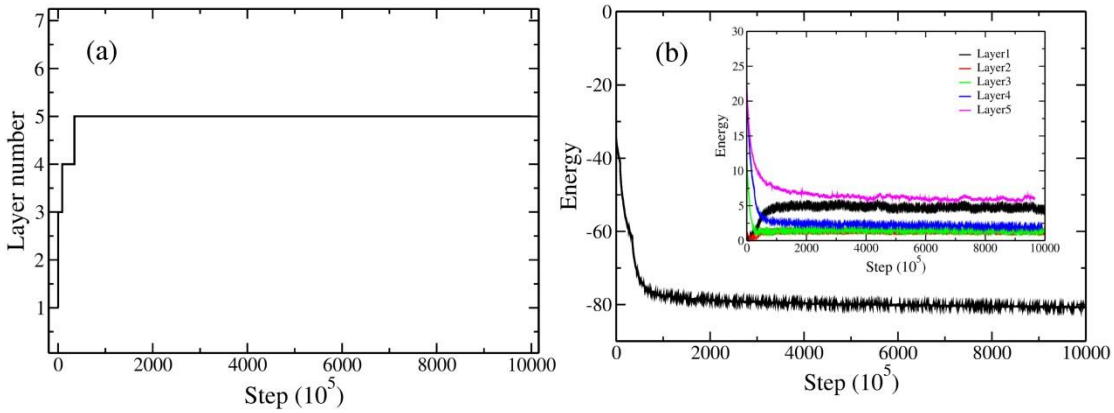

Figure S10. Layer number (a) and total energy (b) versus time.

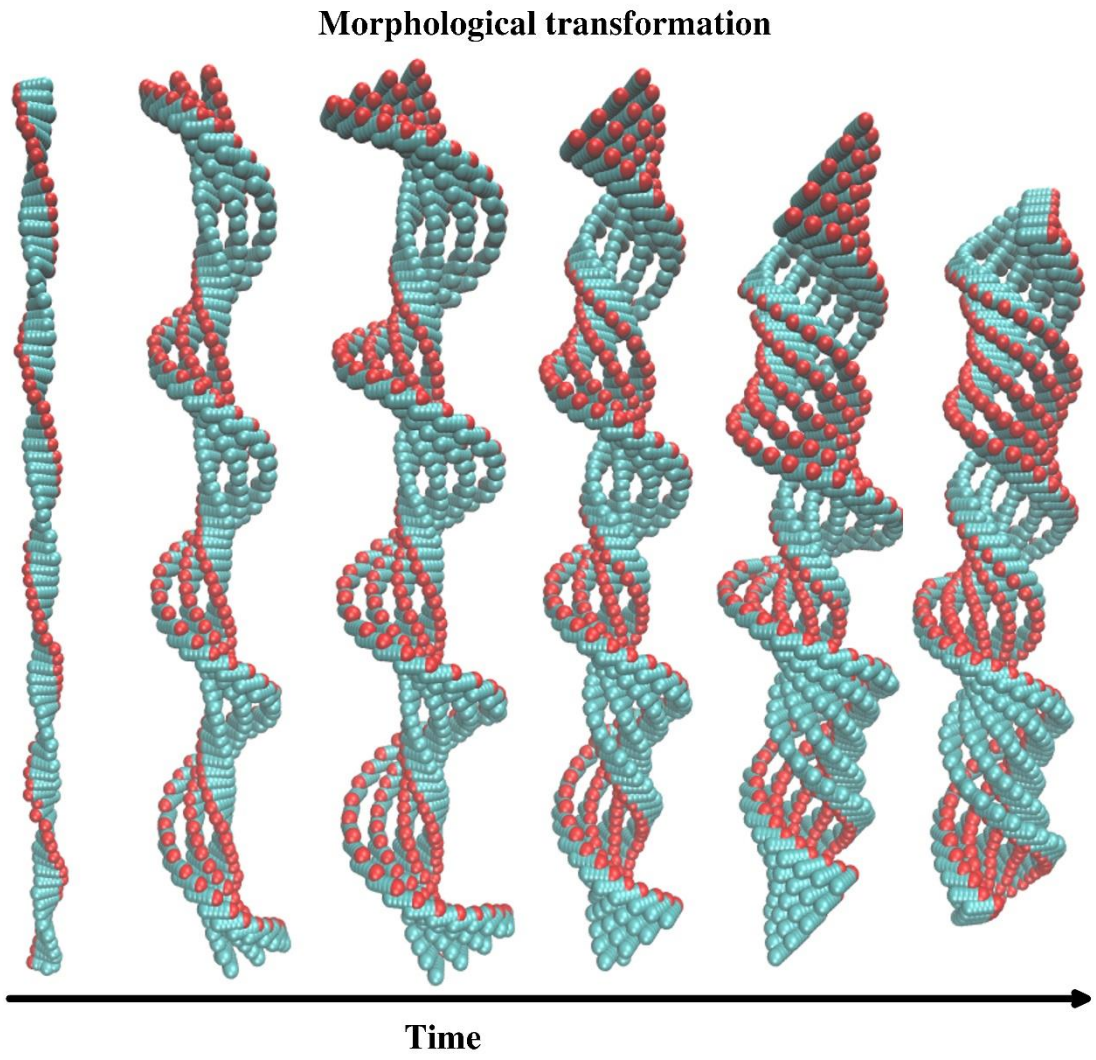

Figure S11. Morphological transformation of KI4K evolving with time.

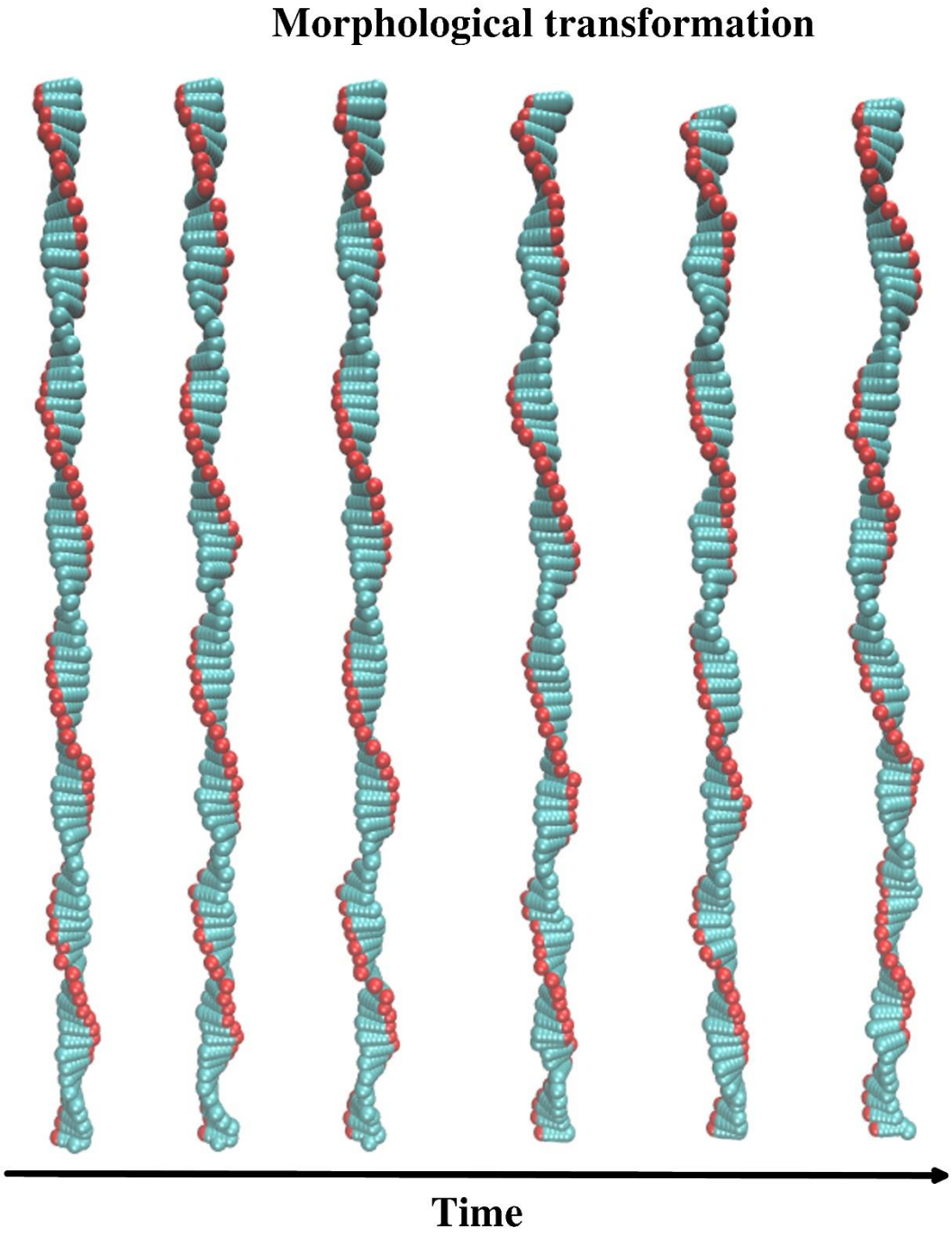

Figure S12. Morphological transformation of I4K2 evolving with time.

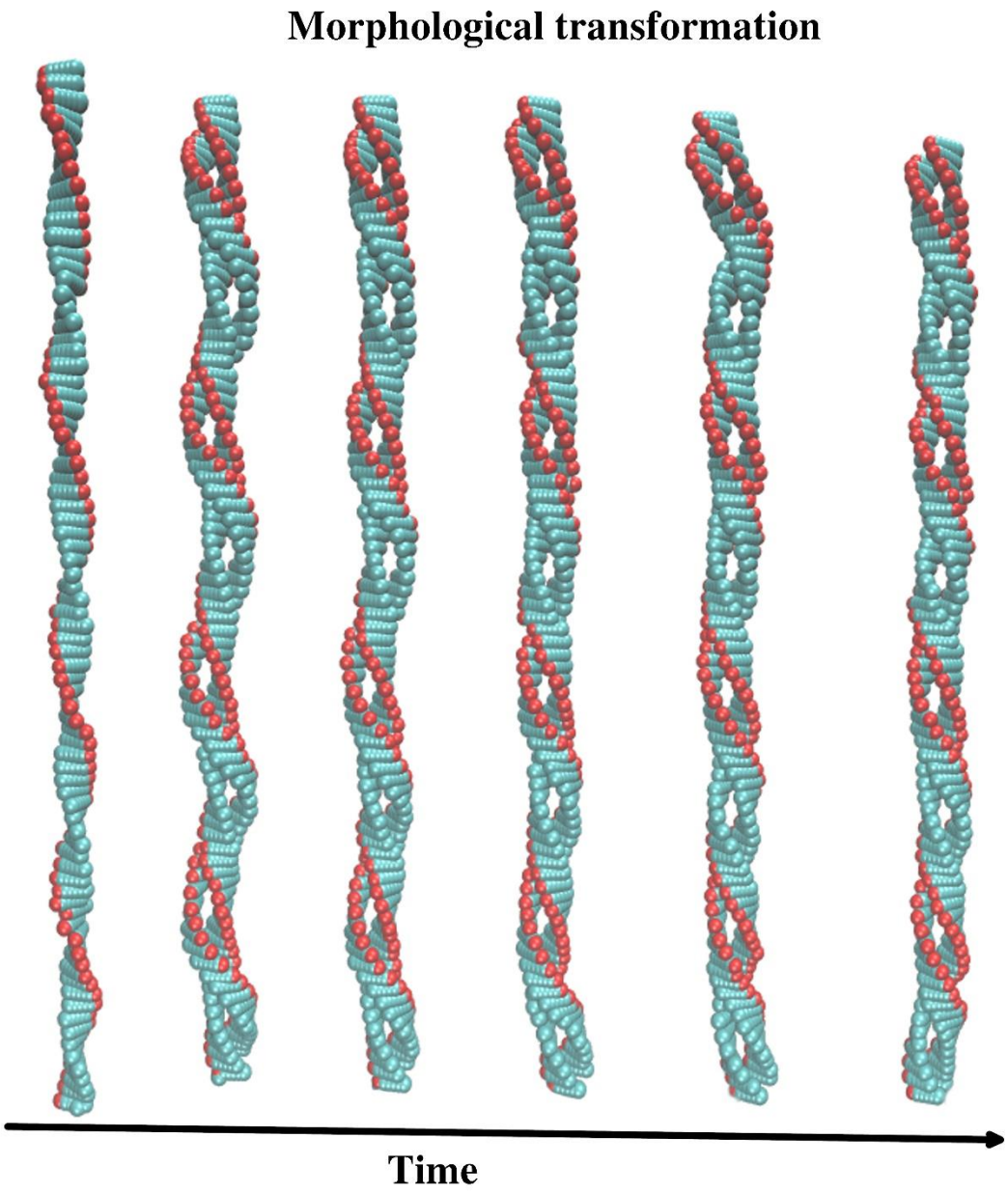

Figure S13. Morphological transformation of a fibril, whose parameters are transformed from those for I4K2, evolving with time.

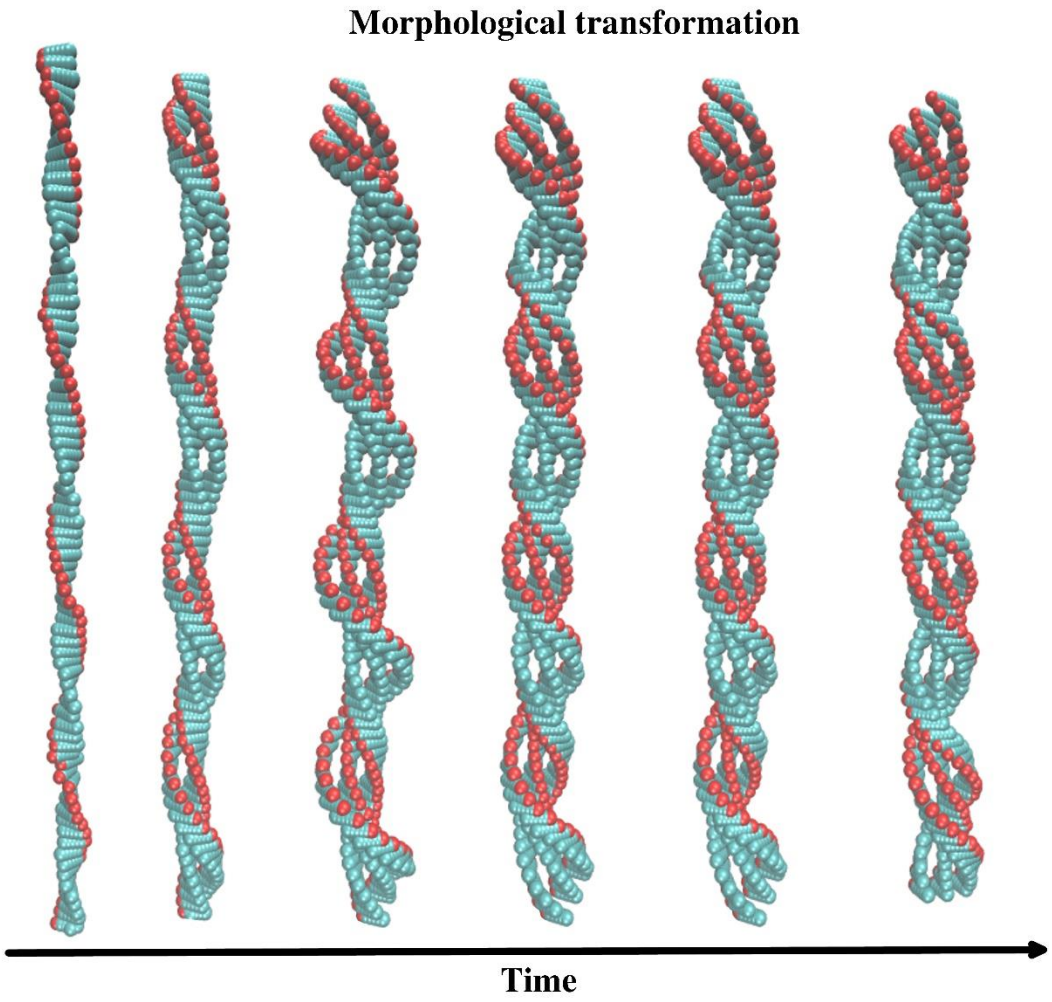

Figure S14. Morphological transformation of a twisted ribbon, whose parameters are transformed from those for I4K2, evolving with time.

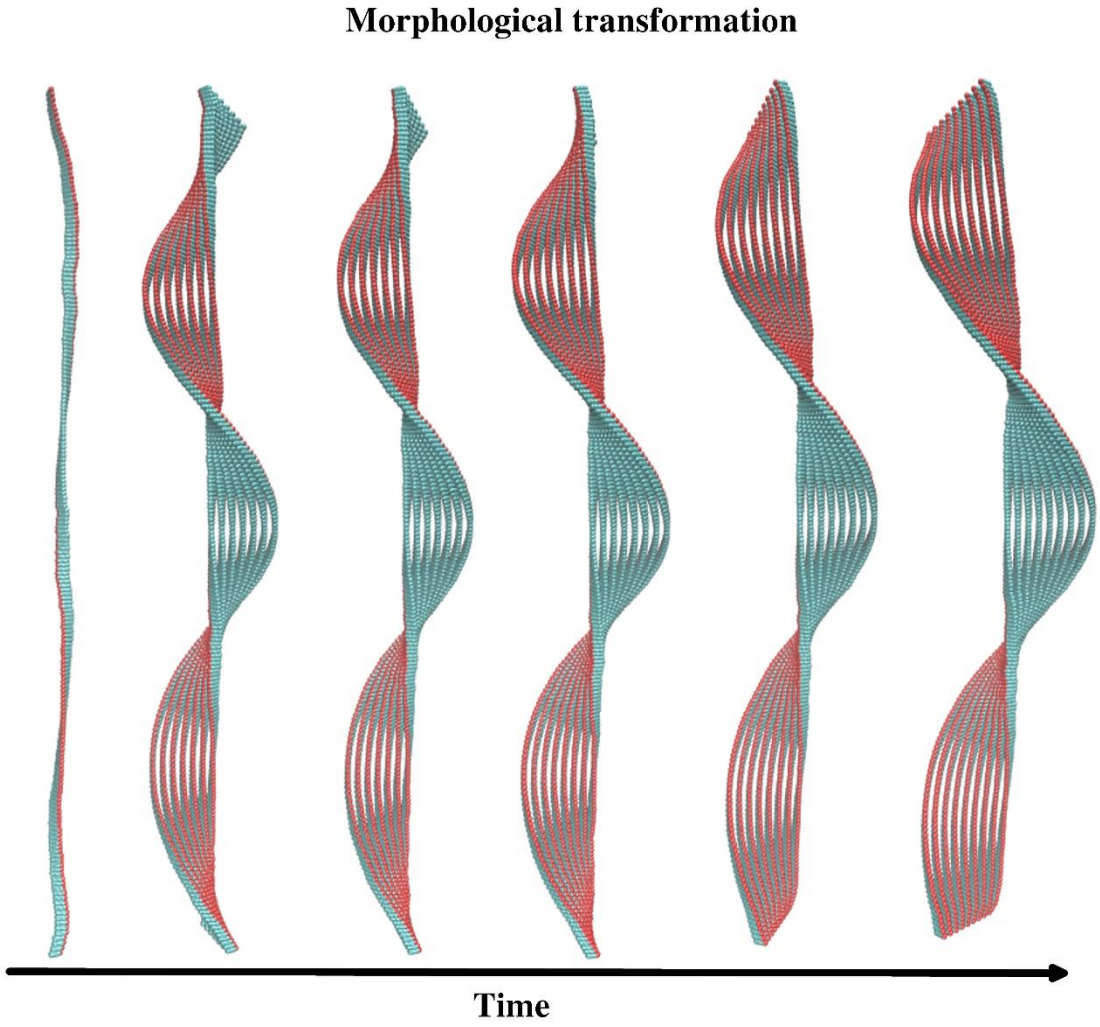

Figure S15. Morphological transformation of a belt, whose parameters are transformed from those for I4K2, evolving with time.